Polymer 309 (2024) 127445

Contents lists available at ScienceDirect

Polymer

journal homepage: www.elsevier.com/locate/polymer

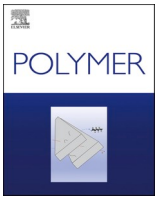

Investigation of thermomechanical behaviors of acrylate-based shape memory polymers by molecular dynamics simulation

Jiaxin Xi [a], Arpit Agrawal [a,b,*], Shima Shahab [a,**], Reza Mirzaeifar [a,1]

[a] Department of Mechanical Engineering, Virginia Tech, Blacksburg, VA, 24061, USA
[b] Lawrence Livermore National Laboratory, Livermore, CA, 94550, USA

ARTICLE INFO

Keywords:
Shape memory polymers (SMPs)
Molecular dynamics (MD) simulations
Crosslinking density

ABSTRACT

Shape memory polymers (SMPs) have received a lot of attention lately due to their potential use as actuators in various applications, including robotics and biomedical device. SMPs are a better choice than other smart materials due to their remarkable ability to recover from significant deformations and their ability to be stimulated remotely. Here, we investigate the mechanical and recovery behaviors of SMPs composed of acrylate-based monomers and crosslinkers with varying crosslink densities, using full-atomistic molecular dynamics (MD) simulations. Physical parameters, such as density and glass transition temperature, are determined for systems with different crosslinking densities. Tensile loading is applied to characterize the mechanical characteristics and shape memory behaviors. Furthermore, the shape-memory behavior of the system with highest crosslinking density is investigated to understand the effects of recovery temperature and deformation temperature on shape recovery. Our findings shed light on the critical structural elements that determine shape recovery ability, giving insights for advanced SMP material design and development. This study adds to our fundamental understanding of SMP behavior and has ramifications for a wide range of technological applications.

1. Introduction

The shape memory effect represents a remarkable property exhibited in certain polymeric materials, allowing them to regain their original shape when exposed to specific stimuli, such as heat, solvent, or focused ultrasound fields [1–3]. Shape memory polymers (SMPs) have emerged as a promising alternative to other shape memory materials like shape memory alloys (SMAs) [4,5] and shape memory ceramics (SMCs) [6,7]. SMPs have found diverse applications across various domains, such as robotics, biomedical devices, smart textiles, and aerospace engineering [8–13]. SMPs offer several advantages that include low density, high frozen strain, cost-effective manufacturing, facile processability, a broad range of shape transition temperatures (T_{trans}), and partial biocompatibility [14–16]. SMPs can be broadly categorized into three main groups based on stimuli to which they respond: chemo-responsive, thermo-responsive, and photo-responsive SMPs [17–20]. Among these, thermo-responsive SMPs that respond to changes in temperature are most widely used. This is primarily due to the ease of regulating the switching temperature and their excellent shape memory behavior. The underlying mechanism behind thermo-responsive SMPs involves heat absorption, which generates molecular motion and modifies stiffness above a transition temperature, leading to shape recovery [21]. One prominent type of thermo-responsive SMPs is the acrylate-based AB copolymer networks, synthesized through the copolymerization of monomers and crosslinkers. The networks in these SMPs offer notable advantages, including biocompatibility [22], relative ease of preparation [23], easy property tailoring [24], and the capability for three-dimensional/four-dimensional (3D/4D) printing [25–27]. The transition temperature range of SMPs, often related to the glass transition temperature (T_g), and their operational attributes, such as deformability and the recovery speed, can be modified by varying the copolymer composition or degree of crosslinking [28–32].

Developing efficient acrylate-based shape memory polymers (SMPs) for remote actuation remains a challenge, particularly achieving full shape recovery within few seconds (<10 s). This is crucial for applications like *in vivo* drug delivery systems induced by high-intensity focused ultrasound (HIFU). While HIFU enables remote and noninvasive actuation of SMPs, current materials exhibit slow actuation and low recovery

* Corresponding author. Department of Mechanical Engineering, Virginia Tech, Blacksburg, VA, 24061, USA.
** Corresponding author.
E-mail addresses: arpitem@vt.edu (A. Agrawal), sshahab@vt.edu (S. Shahab).
[1] This paper is dedicated to the memory of Prof. Reza Mirzaeifar passed away on October 19, 2022.

https://doi.org/10.1016/j.polymer.2024.127445
Received 24 January 2024; Received in revised form 26 July 2024; Accepted 28 July 2024
Available online 29 July 2024
0032-3861/Published by Elsevier Ltd.

percentages [33–36]. To address the issue of recovery, in past, our group investigated the influence of the chemical composition of SMPs on their shape recovery induced by HIFU [36]. SMPs were synthesized using the monomer tert-Butyl acrylate (tBA) and crosslinker di(ethylene glycol) dimethacrylate (DEGMA) [35]. The composition ratio (the ratio of monomer to crosslinker) was tuned to achieve the highest shape recovery ratio (approximately 20% after a continuous 20 s ultrasonic exposure). The introduction of polystyrene (PS) into the tBA-co-DEGMA mixture demonstrated remarkable improvement in shape recovery capabilities; the mixture was able to transition from a deformed shape ($\Delta = 50°$) to the permanent shape ($\Delta = 175°$) within 2 s when subjected to heating via a hair dryer [37]. This shows the potential for tuning both shape recovery and recovery rate by changing the chemical composition that impacts the crosslinking density.

There are numerous types of acrylate polymers and selecting networks through experiments is expensive and time-consuming. Atomistic simulations can accelerate the process at a fraction of cost & time to design the matrix for more efficient SMPs either by screening target materials among numerous candidates or by proposing new combinations of mixture & curing agent tailored to specific properties. Molecular Dynamics (MD) simulations have emerged as a powerful tool to study the connections between the molecular-scale structure and their properties in polymers [38–41]. In our group's previous work, we [38] studied HIFU-induced thermal effect on high and low density polyethylene (PE) using MD simulation and reported that the thermal effect is closely associated with the viscoelasticity of polymer. In another work, MD simulations were conducted to examine the crosslinking mechanism during the curing process of tBA-co-DEGMA (TD)/PS composite [37]. The findings revealed that the inclusion of PS impedes both polymerization and crosslinking processes, hindering the formation of a tightly crosslinked network during the curing process. The shape memory characteristics of various polymers, such as polyisoprene [42], polystyrene [42,43], poly (l-lactide) [44], and epoxy polymers [44,45], have been investigated through atomistic simulations.

As mentioned above, the crosslinking process affects the mechanical and thermal properties of the polymer. The present work investigates the thermo-responsive acrylate-based SMPs (tBA-co-DEGMA) at the atomistic scale. Networks with different crosslink densities are created, and calculations are performed for the T_g, glassy state modulus, rubbery state modulus, and shape recoverability.

2. Materials and methods

2.1. Initial equilibration

The initial tert-Butyl acrylate (tBA) and di(ethylene glycol) dimethacrylate (DEGMA) structures are created by Materials Studio software [46] with consistent valence force field (CVFF) [37,47]. The primary molecular structures of tBA monomer ($C_7H_{12}O_2$) and DEGMA crosslinker ($C_{12}H_{18}O_5$) are schematically represented in Fig. 1. Each cubic simulation box contains 2304 tBA monomers and 216 DEGMA crosslinkers (total 447,552 atoms; more details are shown in Fig. S1), in order to keep the mass ratio of tBA and DEGMA molecules be 85:15 [37]. All Molecular Dynamics simulations in this study are conducted using the LAMMPS software package (Large-scale Atomic/Molecular Massively Parallel Simulator) [48]. This initial large system is created in a low-density configuration to prevent overlaps and is then gradually compressed. Periodic boundary conditions are applied in all directions, and timestep of 1 fs is used. The system's energy (with related to atomic positions) is minimized using conjugate gradient (CG) algorithm. After minimization, an equilibrated structure is obtained by subjecting the system to a series of heating/cooling processes. This begins with equilibrating the system at 298 K for 1 ns using constant pressure and temperature (NPT) ensemble. The temperature is increased to 500 K from 298 K, and then the model is equilibrated at 500 K for 4 ns using NPT ensemble with zero pressure. Next, each model is gradually cooled back to 298 K, and an NPT ensemble is then performed at 298 K for 1 ns. At the end of the relaxation procedure, the side length of each simulation box reaches approximately 168 Å, as shown in Fig. 1c. Models are visualized by Open Visualization Tool (OVITO) [49].

2.2. Crosslinking

Once the initial un-crosslinked system is equilibrated, the crosslinking process starts. Crosslinking procedure is required to create the new bonds and to write the force constants of newly formed bonds. The crosslinking procedure follows an iterative approach involving MD simulations in the LAMMPS code and topology updates in MATLAB, as illustrated in Fig. 2. During the crosslinking stage, un-crosslinked models are crosslinked using the 'fix bond/create' command in the LAMMPS code, a method previously employed in studies [50–52]. Based on our prior work [37], a new bond is formed when the distance between two active sites is less than 4.5 Å. Meanwhile, the new angle and dihedral interactions are also introduced to account for the newly formed bonds.

Within acrylate-based polymer networks, the monomer assumes the role of the soft segment, resulting in shorter chains; the crosslinker is added as the net-point (hard segment), weaving a network structure throughout SMPs. Thus, crosslinking reactions occur between the carbon atoms on the ends of tBA molecule, as shown in Fig. 3a, as well as between the carbon atoms on the ends of tBA molecule and the carbon atoms of the crosslinker DEGMA molecule, as shown in Fig. 3b. It is

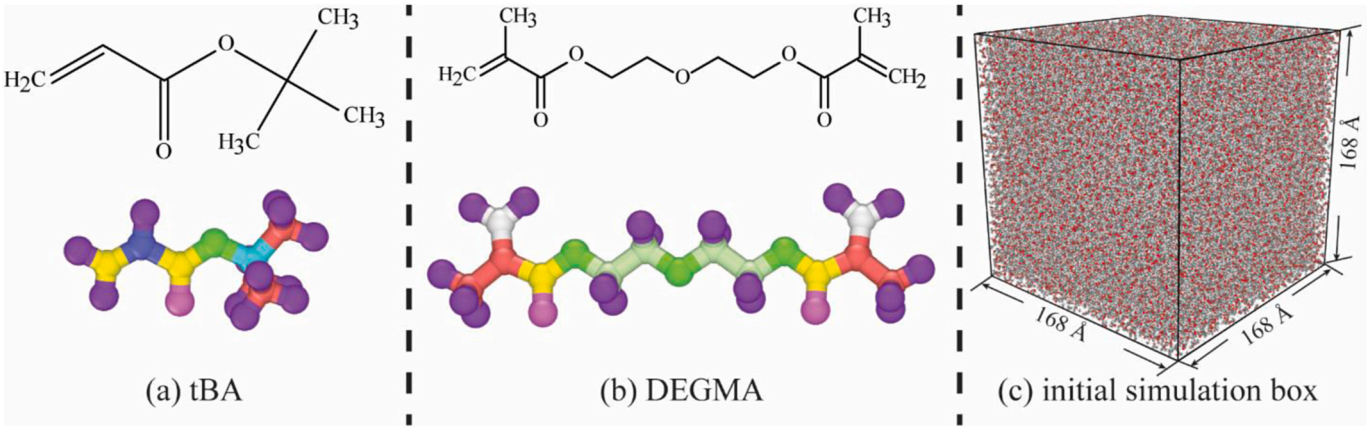

Fig. 1. Molecular structures of (a) tert-Butyl acrylate (tBA), and (b) di(ethylene glycol) dimethacrylate (DEGMA). (c) Initial uncrosslinked model of tBA-co-DEGNA with dimensions of 168 × 168 × 168 Å.

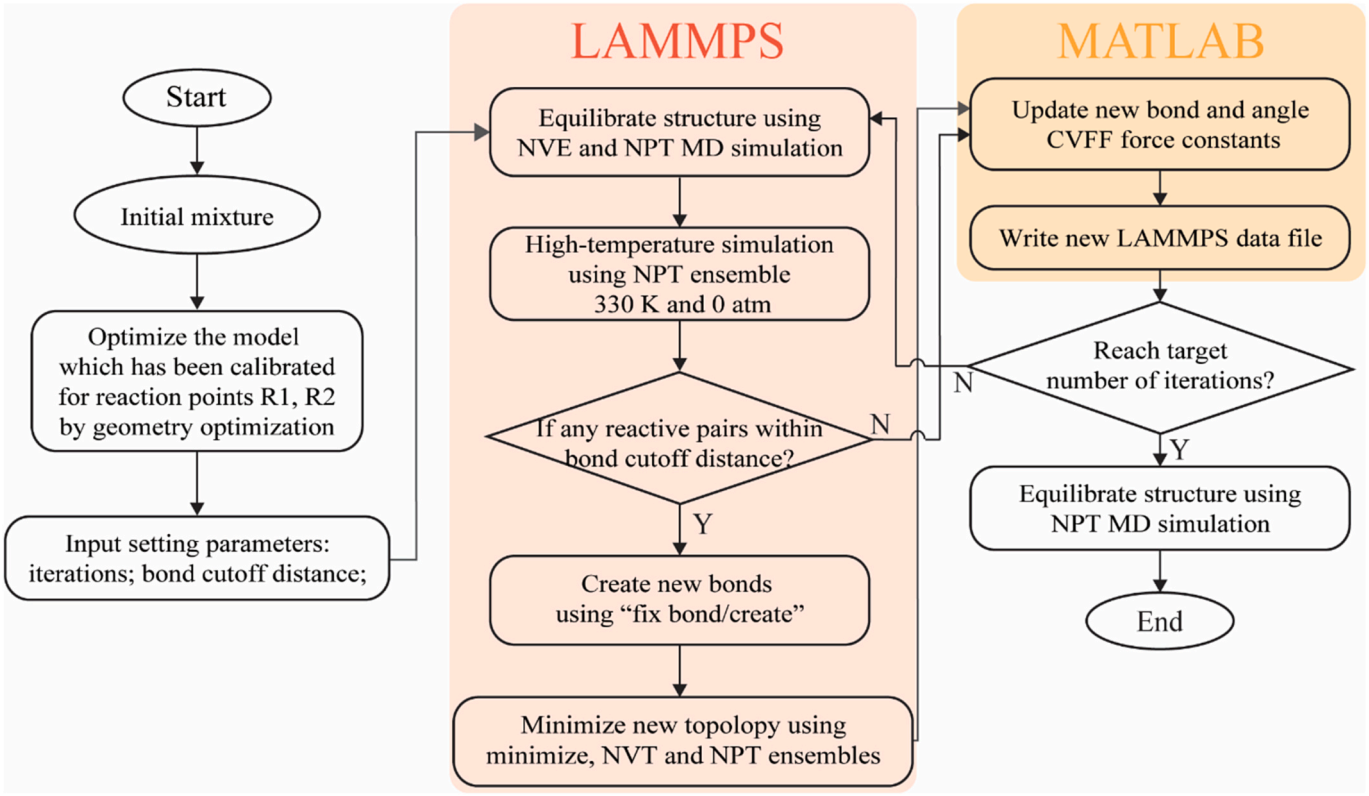

Fig. 2. Summary of process to generate crosslinked acrylate polymer sample.

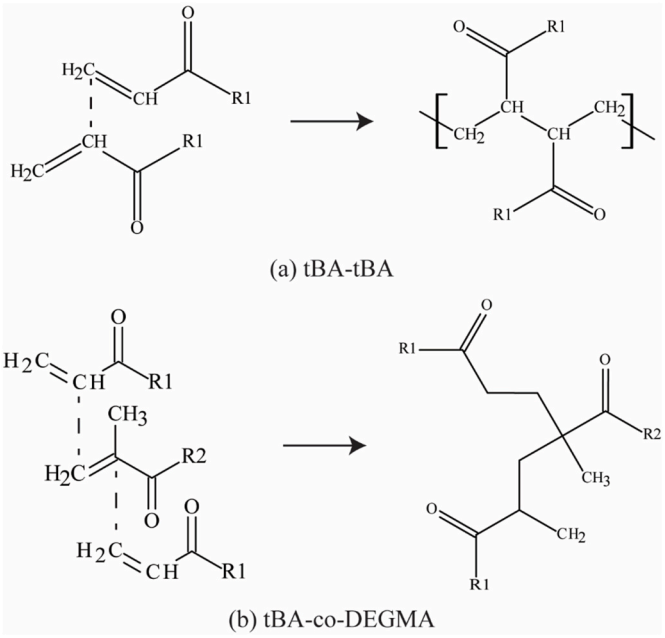

Fig. 3. Schematic representations of (a) a polymerized set of tBA, and (b) a crosslinked set of tBA and DEGMA.

noted that there is one active polymerization site on each tBA molecule and four active crosslinking sites on DEGMA molecule. Importantly, the formation of the new bond is restricted to occurring between molecules of different types.

The atom type of the crosslinked carbon atoms changes after new covalent bonds are formed (changed from "c = " to "c1", "c2" or "c3"). Hence, in the crosslinked network, the atom type of both crosslinked atoms should be updated. In the updated topology, the force coefficients for the new bonds, angles, and dihedrals should be assigned based on the atom type of the newly introduced crosslinked carbon atoms. Besides, the old topology information, which includes the reacted atoms, should also be updated. For instance, before a reaction happens, the carbon atom in tBA molecule forms a bond with one carbon atom (atom type "c = "), and the bond type is "c = -c'". However, after the crosslinking reaction occurred, the bond type changes to "c1-c'" that is caused by the change in atom type from "c" to "c1" (atom type of the reacted atom). Similarly, all other related old topology information, including the angles and dihedrals involving this crosslinked carbon atom is included, should also be refreshed. After the new bonds, angle, and dihedral interactions are created for ten search loops, the CVFF constants are updated, using in-house MATLAB code. The system configuration is then saved, and loops start again.

A crosslinked system is typically constructed at a temperature of 330 K and a pressure of 0 atm. The creation of new bonds, along with the resulting angle and dihedral interactions, triggers a sudden rise in the total energy and internal stress of the systems. To prevent abrupt energy spikes, which may lead to unstable conditions, the system is relaxed after each loop. This relaxation process involves equilibration through both NVT and NPT ensembles. Once the systems attain equilibrium, a new iteration starts again. Overall, we ran a hundred iterations to create new crosslinking networks (new bonds and topology updates). After every ten iterations, CVFF constants are updated using in-house MATLAB code. Systems with updated CVFF constants are saved, resulting in ten systems with increasing crosslinking densities. These ten systems, along with the uncrosslinked system, were utilized to study the impact of crosslinking on various properties.

2.3. Glass transition temperature (T_g)

After the crosslinking process, all 10 crosslinked systems undergo energy minimization and are subsequently equilibrated for an additional

0.5 ns using an NPT ensemble, maintaining a temperature of 600 K and a pressure of 0 atm. Then, the T_g is determined by analyzing the changes in the mean square displacement (MSD) of polymer chain atoms. The MSD curves are derived using the following formula:

$$\mathrm{MSD} = \frac{1}{N}\sum_{i=1}^{N}\left(r_i(t) - r_i(t=0)\right)^2 \quad (1)$$

where the $r_i(t)$ is the mass center of the position of particle i at time t, $r_i(t=0)$ is the reference position of atom i, and N is the total number of atoms in the simulation box. As the temperature decreases, the MSD values of the NPT ensemble are recorded at intervals of 10 K, each for a duration of 1000 ps, as shown in Fig. 4b. The T_g is identified as the point at which a pronounced gap emerged between the MSD curves.

The second approach involves determining the T_g by gradually cooling down all 10 crosslinked systems at a rate of 0.050 K/ps until reaching a temperature of 150 K, as shown in Fig. 4d. Throughout this cooling process, the density is monitored as a function of the temperature. The T_g is determined by identifying the intersection point of two lines representing the glassy and rubbery regions. These lines are identified using a piecewise linear regression model.

2.4. Mechanical properties

Once the T_g is determined for all 10 systems with varying crosslinking density, the material properties for the glassy (room temperature, 298K) and rubbery (high temperature, 400 K (~30 K above T_g) states are computed. The stress–strain relationship of each system is established through tensile loading conducted along the z-direction, as shown in Fig. 4c. For deciding the strain rate, five strain rates are simulated: 1e10/s, 5e09/s, 1e09/s, 5e08/s, and 1e08/s, which are frequently used in MD simulations [53–60]. The resulting stress-strain curves are shown in Fig. S4 in the Supplementary document. The resultant stress-strain curves show that there is no significant behavior change between 1e09/s, 5e08/s and 1e08/s. Thus, each system is deformed at the constant strain rate of $5 \times 10^8\ s^{-1}$ under an NPT ensemble for both temperatures, employing a time-step of 1 fs. Throughout the loading, a zero-pressure boundary condition is applied in the other two dimensions of the simulation box.

2.5. Shape memory behavior

To understand the factors influencing the shape memory behaviors, a thermo-mechanical loading cycle is implemented within the simulations, as illustrated in Fig. 5, and has following steps.

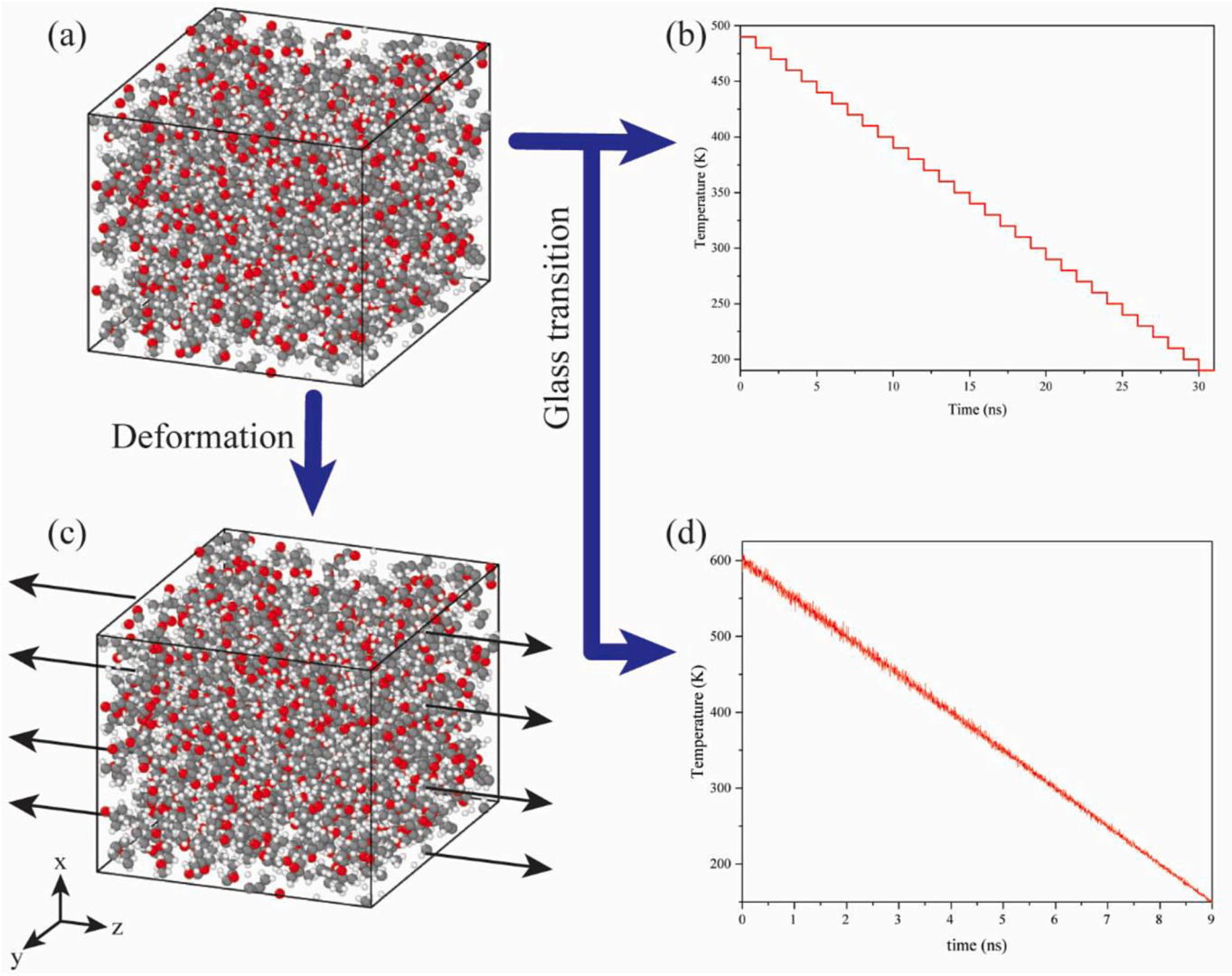

Fig. 4. (a) The schematic diagrams of crosslinked system. Schematic description of (b) stepwise and a (d) continuous cooling to determine the T_g. (c) Molecular model for uniaxial tensile deformation.

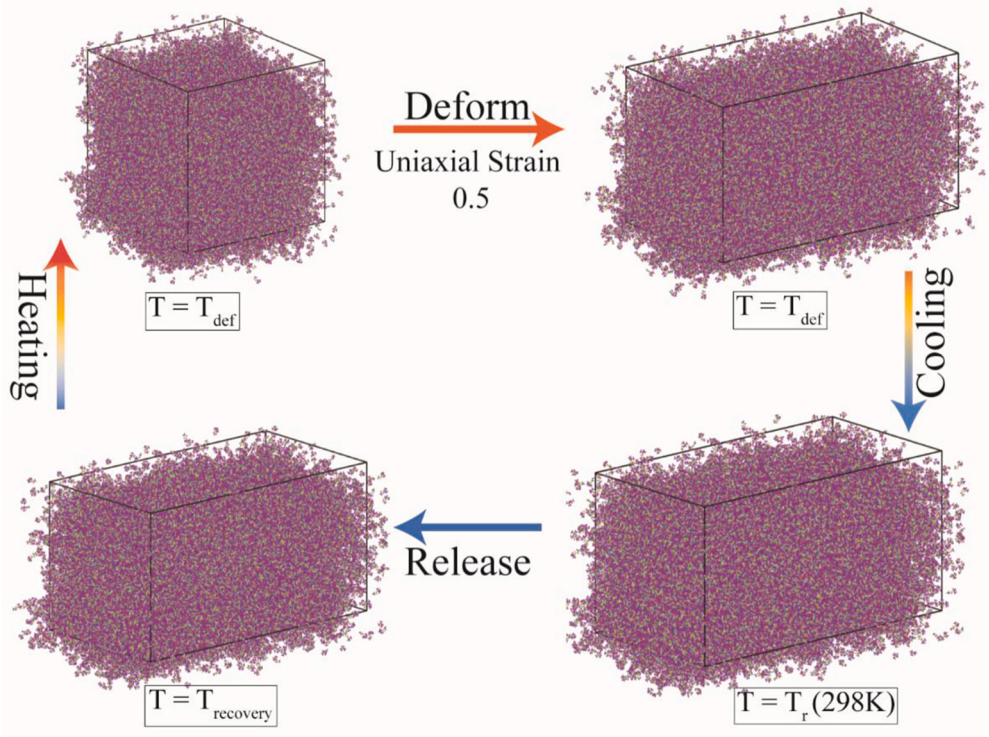

Fig. 5. Schematic thermomechanical loading conditions for shape recovery.

(a) Rapidly heating the highest crosslinked structure (crosslinking density = 62.7 %) obtained from section 2.2 from room temperature (T_r = 298K) to the deformation temperature (T_{def}) (that is above T_g).
(b) Maintaining the temperature at T_{def} for 0.4 ns.
(c) Subjecting the sample to stretching with the strain up to 0.5 (ε_d = 0.5) at T_{def}, with a rate of $1 \times 10^{10}\ s^{-1}$.
(d) Allowing for an NVT isochoric relaxation for 0.4 ns at T_{def}.
(e) Cooling from T_{def} to T_r.
(f) Keeping the temperature constant at T_r for 0.2 ns using the NVT ensemble.
(g) Unloading the sample and releasing stress with the NPT ensemble for 0.5 ns at a temperature of T_r.
(h) Reheating the system from T_r to the recovery temperature ($T_{recovery}$).
(i) Conducting NPT deviatoric relaxation at $T_{recovery}$ for 0.5 ns, which serves as the recovery step.

The heating and cooling rates of 0.5 K/ps are used in each heat and cooling step, respectively. It should be noted that the strain rate of $1\times 10^{10}\ s^{-1}$ used in deformation step (c) is higher than the strain rate used in section 2.4. The strain rate for the shape memory polymer deformation process is intentionally faster to achieve results more quickly. It is important to note that the simulations discussed here are independent of those described in sections 2.4, focusing specifically on the shape memory behavior under specific conditions. The changes of the strains in the cycles are recorded and the recovery ratio (R_r) is defined as $R_r = \frac{l_p - l_r}{l_p}$, where l_p and l_r are the length of specimen cube in its permanent and recovered shapes, respectively.

3. Results and discussions

3.1. Crosslinked modeling

After polymerization, measuring the degree of crosslinking is essential to verify the effectiveness of the crosslinking algorithm. Crosslinking density refers to the ratio of bonds formed at particular iteration to the total possible bonds in the system. As shown in Fig. 6a, within acrylate-based polymer networks, the monomer assumes the role of the soft segment that results in shorter and less bulky chains. This increases the mobility of the molecular chains and facilitates easier deformation especially when the material shifts from rigid plastic at room temperature to soft rubber above its T_g. Concurrently, the crosslinker serves as a net-point, weaving a network structure throughout SMPs.

The crosslinking process is iterated up to 100 times, with the quantity of crosslinking recorded every 10 iterations. After the crosslinking process begins, the simulations continue until either the system runs through the predetermined 100 iterations, or all activated reactive sites can be crosslinked. As depicted in Fig. 6b, the tBA-co-DEGMA system achieves its maximum crosslink density of 62.7% in the allotted number of repetitions.

3.2. Glass transition temperature

Thermal transitions are significant in the development and use of thermal-responsive SMPs and are also crucial for validating the computational model. When the temperature increases, the polymer transforms from a rigid solid, which exhibits minimal deformation under external forces, to a highly elastic state with a significant increase in deformation capacity. T_g is calculated by measuring the changes in MSD and the density of SMPs.

MSD measures the deviation over time between a particle's position and its initial position, serving as a common method for assessing the random mobility of atoms within a system. MSD curves are generated for the system with highest crosslinking (iteration = 100) at different temperatures to characterize thermal motion, as shown in Figs. 7a and S2. As temperature increases, MSD values rise continuously, because of the thermal motion of the molecules; moreover, these values gradually increase over time. As temperature increases, MSD values exhibit a continuous increase owing to the thermal agitation of molecules. MSD

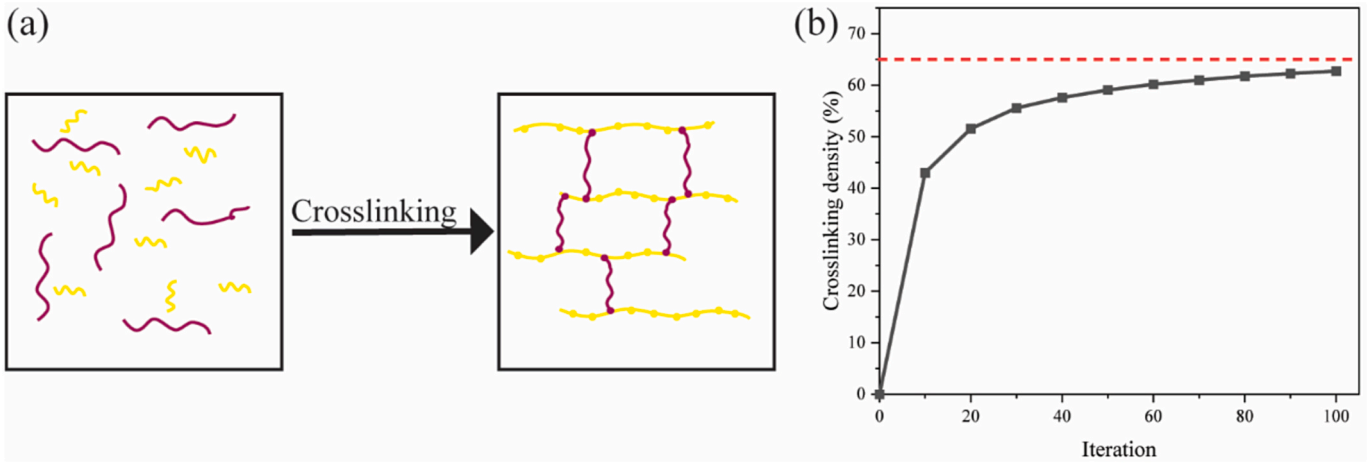

Fig. 6. (a) Schematics of polymerization and crosslinks of tBA (monomer) and DEGMA (crosslinker) mixture before and after the crosslinking process. (b) Crosslinking density across iterations from 0 to 100.

values increase with time for given temperature till equilibration. During the transition from a glassy to a rubbery phase in polymers, the interplay of torsional and rotational motions alongside local mobility facilitates chain disentanglement, culminating in a sudden surge in diffusivity. This abrupt spike in diffusivity manifests as a sharp ascent in the MSD curves plotted against time elapsed. By scrutinizing the

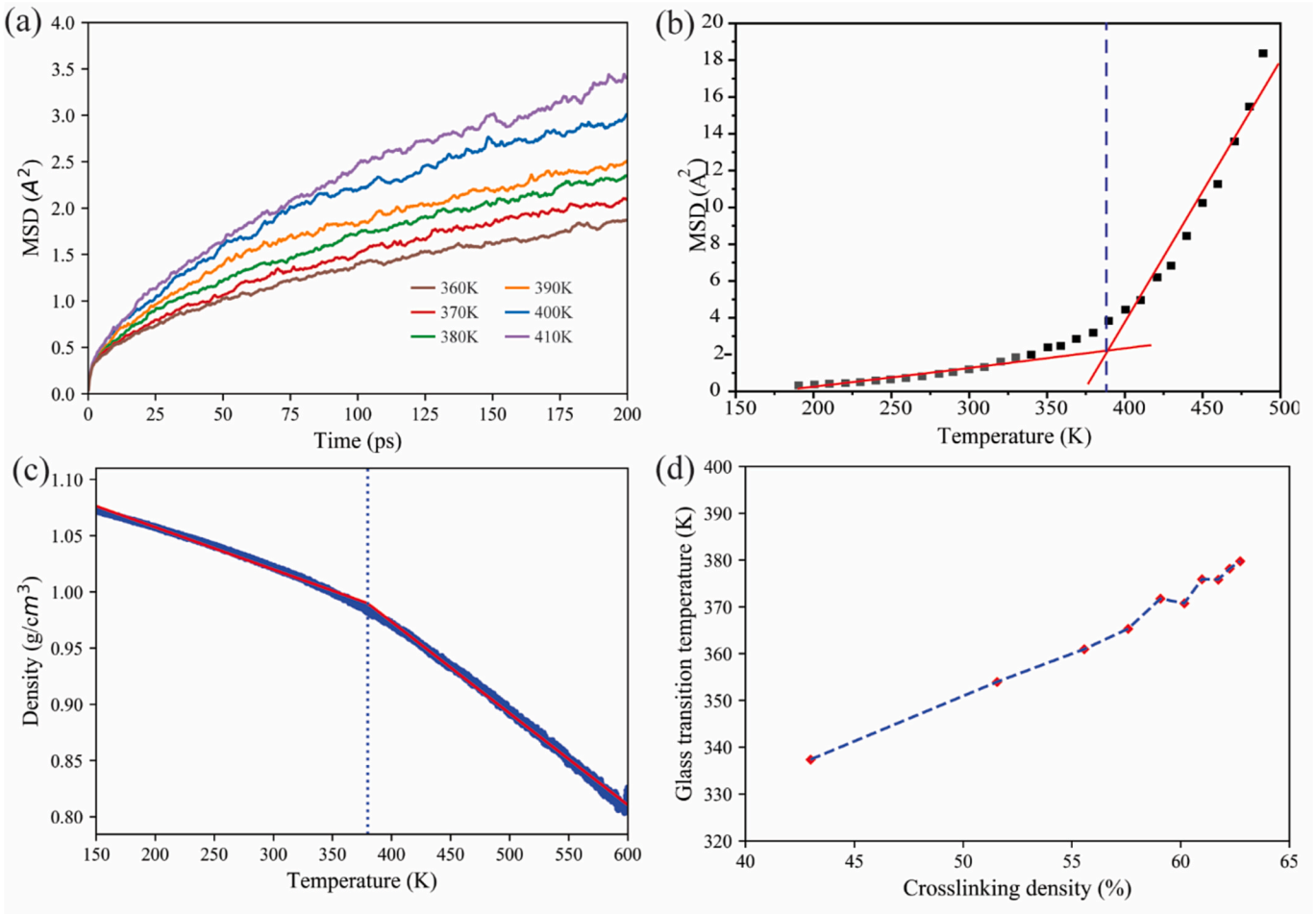

Fig. 7. (a) MSD curves for the highest crosslinked system (crosslinking density = 62.7 %) at various temperatures. (b) MSD of the structure as a function of temperature for the highest crosslinked system (crosslinking density = 62.7 %) at 200 ps. Intersecting point of fit of two linear regression lines is noted as T_g. (c) Density as a function of temperature (blue line) for the system with the highest crosslinked (crosslinking density = 62.7 %). The straight-line fits (red lines) of the glassy and the rubbery density versus temperature is shown. The T_g for this case is determined to be 379.8K. A similar analysis is done for the other 9 systems with different crosslinking densities, as shown in Fig. S3. (d) The T_g values for different crosslinking densities. (For interpretation of the references to colour in this figure legend, the reader is referred to the Web version of this article.)

intervals between individual MSD curves, a rough estimate of the glass transition temperature within a 10 K range can be derived. In Figs. 7a and S2, a clear distinction in the mobility of chain segments is evident between lower temperatures (not exceeding 390 K) and higher temperatures (not falling below 400 K). This abrupt transition between the two temperature ranges is further highlighted in Fig. 7b, where the MSD is re-plotted against temperature at 200 ps. Notably, the T_g is observed to be around 390 K. To determine the optimal fit curve, an iterative procedure employing the piecewise linear function along with "orthogonal distance regression" algorithms [61,62] is used.

The second method, the expansion method, uses the fact that the glass transitions are second-order phase transition, where thermal expansion coefficient changes abruptly before and after T_g. It is commonly understood that during the glass transition of polymers, molecular motion facilitates the disentanglement of chains. Consequently, there is an increase in thermal expansion exhibited by the polymers. This increase in thermal expansion manifests as a sudden rise in volumetric properties. By examining the shifts in density with temperature, one can approximate the value of the glass transition temperature. This method can be considered more accurate than the first method (using MSD) as it depends on the physical quantity of the system that can be also measured in experiments. This method has been used in multiple previous works [63–66]. Here, the temperature of systems is decreased with varying crosslinking densities from 600 K to 150 K at a cooling rate of 0.050 K/ps under isobaric conditions (NPT ensemble). The recorded density for each system is plotted against the temperature, as shown in Fig. 7c (for crosslinking density = 62.7 %) and **S3** (for other different crosslinking densities system). It is evident that for all the systems, density decreases with increase in temperature, and a change in slope is observed. The thermal expansion coefficient is proportional to the slope and the temperature where the slope changes correspond to T_g.

The change in the slope (at T_g) indicates transition from a glassy state (where chain segment motion is restricted) to a rubbery state (where chain segments gain flexibility). T_g is estimated with piecewise linear regression for all 10 systems. For example, Fig. 7c determines T_g of the system that has highest crosslinking density (crosslinking density = 62.7 %) as 379.8 K. In experiments, our group obtained T_g value between 60 and 80 °C (from 333.15 to 353.15 K) for the same system [37]. The simulated cooling rate is at least several orders of magnitude faster than achievable in any experiment, leading to a shift in T_g towards higher values. This phenomenon has also been observed in previous studies [67,68] and is primarily due to logarithmic cooling rate dependence. The difference between MD simulations (crosslinking density = 62.7 %) and experiments (crosslinking density in experiment is not known) is around 5.66 % indicates that the current model and crosslinking process in MD simulations are capable of predicting T_g of polymer systems.

Fig. 7d shows increase in T_g with increase in crosslinking density (or iteration). A similar trend has been reported in previous studies [69–72]. In highly crosslinked networks, where the number of monomers between crosslinking points decreases, T_g can reach substantially higher values in comparison to the non-crosslinked system. This increase is attributed to the establishment of a more compact model structure with a larger relative molecular mass in high crosslinking models. This hinders the free movement of molecular chains, resulting in an elevated T_g. Furthermore, a higher crosslinking density intensifies the hindrance to molecular chain movement. An increase in crosslinking implies that the transition has to change the property of a larger number of bonds, angles, etc., which increases the required energy and thus increases T_g.

3.3. Mechanical behavior

The influences of the crosslinking density and temperature (above and below T_g) on the mechanical properties of tBA-co-DEGMA SMP are investigated. All 10 crosslinked systems are deformed at room (298 K) and high (400 K) temperatures, with a constant strain rate $5 \times 10^8\ s^{-1}$. Fig. 8a–**S5, and S6** present the typical stress–strain curves of the tBA-co-DEGMA SMP with different crosslinking densities at room (298 K) and high (400 K) temperatures, respectively. These trends are manifested in the strength and Young's modulus through the calculation of the slope of the linear segment of the curves. The increase of corresponding properties for each state is illustrated in Fig. 8b and d.

Fig. 8b shows that Young's modulus increases from 215 MPa to 1350 MPa, while the yield strength increases from 11 MPa to 73 MPa at about 8 % strain, with the crosslinking density increase from 0 % to 43.0 %. Furthermore, Young's modulus continues to rise to 1600 MPa, and yield strength increases to 88 MPa reaching the highest crosslinking density at room temperature. This implies that the Young's modulus and the yield strength gradually increase as crosslinking density increase in glassy (below T_g) state. This aligns with the usual pattern observed in polymeric systems, where highly crosslinked systems demonstrate a greater capacity to bear loads compared to systems with lower levels of crosslinked [73]. Experimentally, the tBA-co-DEGMA yields at a stress of 10.5 MPa, then breaks at ~0.3 strain; and the young's modulus is 270.12 MPa [37]. Each experimental value is less than those from MD simulation, because the strain rate in MD simulation is at ten orders of magnitude higher than those in experiments. By using a linearized Eyring-like model, Fig. S7 shows that the Young's modulus values predicted by MD simulation align well with the experimental data. Therefore, the MD simulation results can be considered reliable for predicting the mechanical properties of copolymers, based on the agreement between the simulation and experimental outcomes. More detail can be found in Fig. S7 of the Supplementary document.

Similarly, Fig. 8d displays that as the crosslinking density increases from 0% to 43.0%, Young's modulus increases from 29 MPa to 160 MPa, and the yield strength increases from 2.9 MPa to 8.1 MPa at about 8% strain. Subsequently, Young's modulus continues to increase by approximately 700 MPa, and yield strength reaches 35 MPa at the highest crosslinking density at 400 K. This highlights a gradual augmentation in Young's modulus and yield strength with increasing crosslinking, particularly in the rubbery state (above T_g). On the other hand, comparing Fig. 8a and **c,** the tBA-co-DEGMA exhibits reduced mechanical properties at 400 K compared to the room temperature, and the yielding point becomes less distinct. Young's modulus decreases to ~700 MPa from 1600 MPa for the same crosslinking density tBA-co-DEGMA, and the yielding point becomes less clear.

Furthermore, at room temperature, the stress curves show an increase with higher strain until reaching the yield point. Subsequently, stress undergoes a decline. More details are explained in Fig. S8. However, no significant stress decrease is observed in the stress-strain curve at 400 K. This observation is rational as chain mobility increases at higher temperatures, facilitating easier deformation. Conversely, the melting of the crystalline phase can also contribute to reduced stiffness and strength. Supporting this, Peng et al. [40] reported that 10 nm amorphous Polyethylene (PE) nanofibers below the T_g exhibited more pronounced necking after reaching the yield point compared to results above the T_g, leading to stress decrease.

3.4. Shape memory behavior

The effects of recovery and deformation temperature on shape memory performance are studied. A basic form of shape memory effect in SMPs is shown in Fig. 5. As shown, the polymer samples are first heated to a deformation temperature (T_{def}). Samples are subsequently loaded at T_{def}. After the loading, samples are cooled down to room temperature. After unloading, samples have fixed deformed/temporary shape at room temperature which finishes the shape fixing step for SMPs. Original shape can be recovered from deformed/temporary shape by heating the sample at $T_{recovery}$. In most of the cases, both T_{def} and T_r are more than T_g (thus T_g is also called shape memory transition

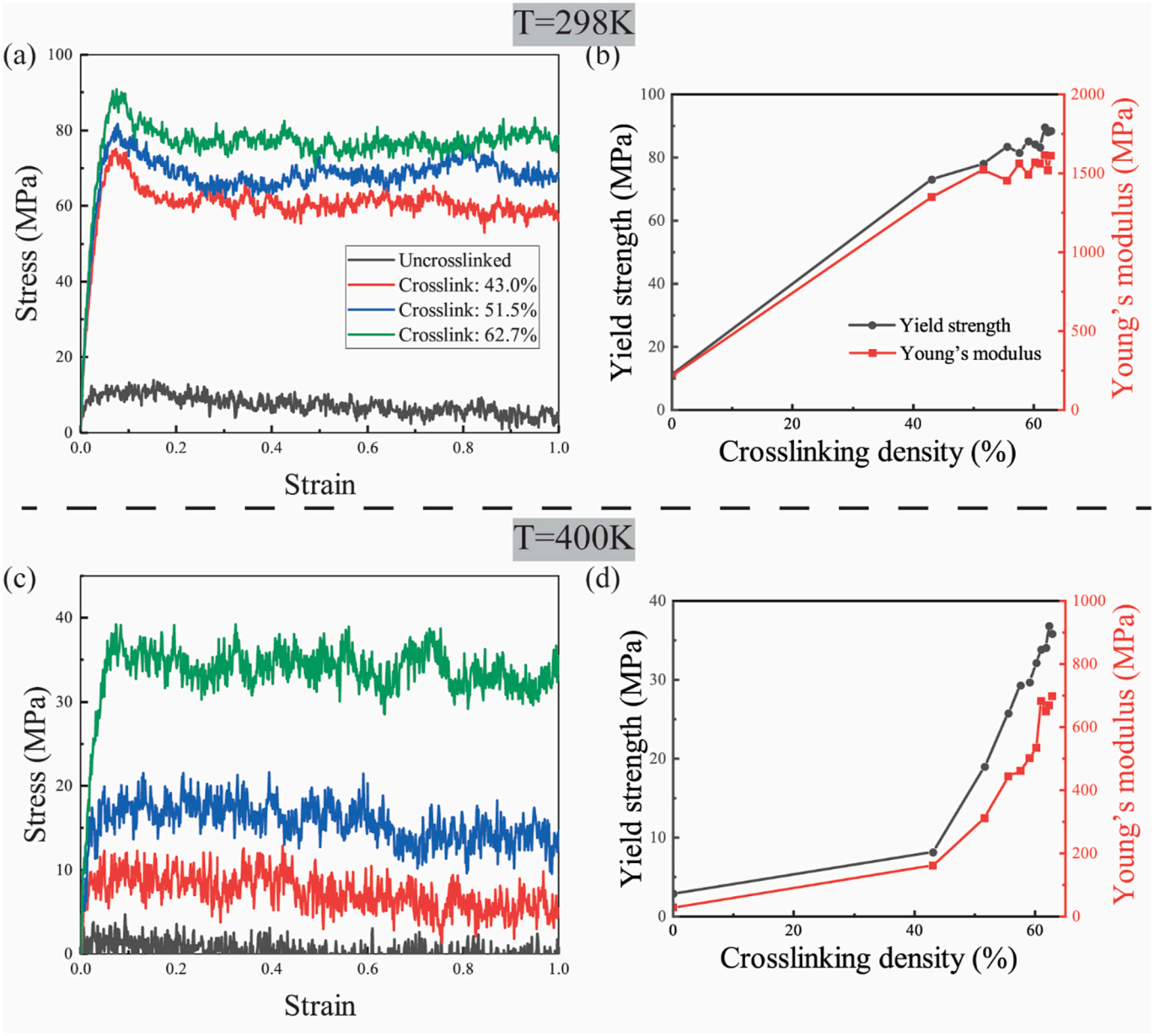

Fig. 8. (a) Stress–strain curves obtained at tensile deformation of un-crosslinked and crosslinked systems with crosslinking densities of 43.0 %, 51.5 % and 62.7 % at room temperature (T = 298 K). (b) Yield strength (black) and Young's modulus (red) with different crosslinking densities at room temperature (glassy state). (c) Stress–strain curves obtained at tensile deformation of un-crosslinked and crosslinked systems with crosslinking densities of 43.0 %, 51.5 % and 62.7 % at high temperature (T = 400 K). (d) Yield strength (black) and Young's modulus (red) with different crosslinking densities at high temperature (rubbery state). (For interpretation of the references to colour in this figure legend, the reader is referred to the Web version of this article.)

temperature, T_{trans}). As shown in section 3.2, T_g can be modified by changing the degree of crosslinking thus modifying the required T_{def} and $T_{recovery}$. In this section, we show the impact of T_{def} and $T_{recovery}$ on shape memory behavior of system with highest crosslinking density.

In the deformed/temporary state, a considerable internal stress is stored within its crosslinking structure. Heating the structure above T_{trans}/ T_g releases this accumulated stress and original shape can be obtained again. In experiments, slightly high temperature (~+10 K) is used for recovery of the polymer, but these experimental temperatures cannot cause notable recovery in atomistic simulations due to difference in timescale (~ nanosecond runs in simulations) [74]. Recovery in the atomistic simulations can be accelerated by using higher temperatures than experiments. Here, we increased T_{def} and $T_{recovery}$ incrementally by 20, 40, and 80 K higher than T_g. Since $T_{recovery}$ needs to be higher than the T_{def} , this results in total six conditions. The changes of strain in tBA-co-DEGMA SMP with the highest crosslinking density during the shape recovery process are recorded as shown in Fig. 9. Strain recovery rates for six different conditions are shown and the recovery speed depends on the deformation temperature and recovery temperature.

Fig. 9a reported that when $T_{def} = T_g + 20$ K, raising the $T_{recovery}$ would progressively enhance the R_r parameter (as mentioned in **section 2.5**) from ~3 % to ~ 5.5 % and ~8 % for $T_{recovery}$ increased from 20 to 40 and 80 K. Fig. 9b shows that when $T_{def} = T_g + 40$ K, $T_{recovery}$ shows an insignificant effect on R_r. Moreover, comparing Fig. 9c, when using the same $T_{recovery}$, the smaller the T_{def} used, the larger the R_r shows. In conclusion, increasing the $T_{recovery}$ and decreasing T_{def}, increases the R_r. A similar phenomenon was reported in previous studies, including both experimental observation [75] and simulation works [76,77]. Abberton et al. [77] suggested both T_{def} and $T_{recovery}$ between 1.27 T_g and 1.90 T_g to achieve the best shape recovery performance.

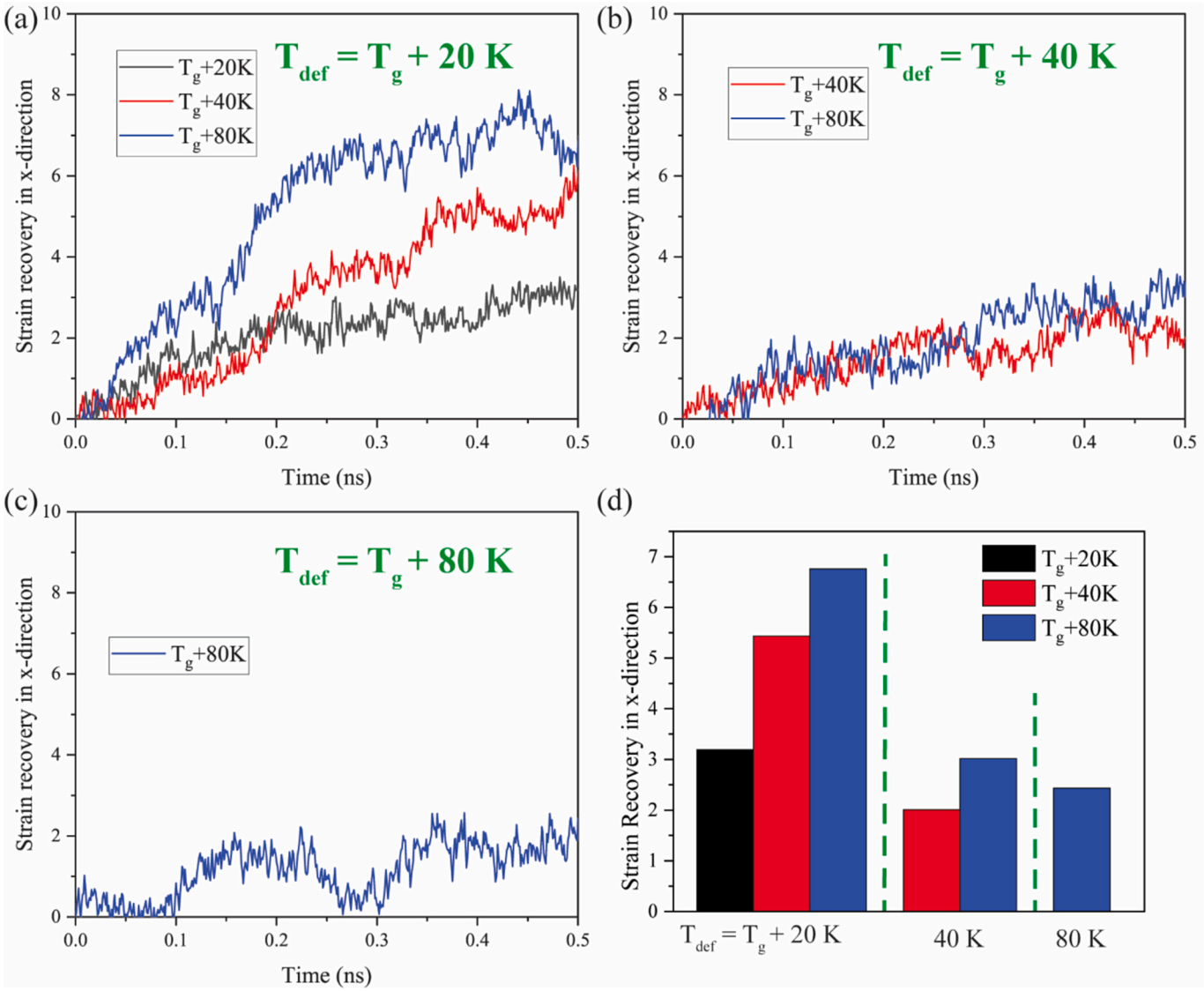

Fig. 9. Evolution of stretch recovery for highest crosslinking density system at deformation of (a) $T_g + 20$ K, (b) $T_g + 40$ K, and (c) $T_g + 80$ K and at different recovery temperatures (black line: $T_g + 20$ K, red line: $T_g + 40$ K, and blue line: $T_g + 80$ K).(d) Strain recovery in 0.5 ns with different deformation and recovery temperatures. (For interpretation of the references to colour in this figure legend, the reader is referred to the Web version of this article.)

To better understand the effect of $T_{recovery}$, we considered potential energy, as shown in Fig. 9. At the same relative T_{def}, the potential energy in the final period at higher $T_{recovery}$ is also higher than at lower temperature. This difference is the source of the difference in the simulation system's R_r. On the other hand, decreasing T_{def}, increases the R_r at the same $T_{recovery}$. This is due to the significant plastic deformation observed at the net points and/or the occurrence of nonreversible flow within the segments as the T_{def} rises. When deformation is done at or a little above the T_g , the material is in a state where it can undergo significant rearrangement without permanent plastic deformation. This means that any deformation incurred is reversible, leading to enhanced shape recovery during subsequent heating cycles.

4. Conclusions

In this work, molecular dynamics (MD) simulations are used to study acrylate-based shape memory polymer system (tBA-co-DEGMA) with various crosslinking densities. A crosslinking technique is introduced to build a series of systems with different crosslink densities; several key properties of this material, including thermomechanical property (glass transition temperature), mechanical property (Young's modulus and yield strength) and shape memory properties are studied. The results from the MD simulations show that an increase in crosslinking density can cause the increase in T_g, as well as Young's modulus, and yield strength in both the glassy and rubbery states. Furthermore, the effect of recovery temperature and deformation temperature are investigated. Using the same recovery temperature, the smaller the deformation temperature used, the larger the recovery ratio shows. The findings reveal that SMPs exhibit ideal shape deformation at low temperatures and efficient shape recovery at high temperatures. We expect that this research will be useful in custom-designing new stimuli-responsive materials as well as in gaining a deeper knowledge of the microstructure dependent thermo-mechanical behavior of shape-memory polymers. Future simulation work can build on these results to examine the effects of filler particles and to test HIFU-responsive on the SMP behavior.

CRediT authorship contribution statement

Jiaxin Xi: Writing – review & editing, Writing – original draft,

Methodology, Investigation, Conceptualization. **Arpit Agrawal:** Writing – review & editing, Writing – original draft, Methodology, Conceptualization. **Shima Shahab:** Writing – review & editing, Supervision, Methodology, Investigation, Funding acquisition, Conceptualization. **Reza Mirzaeifar:** Supervision, Methodology, Investigation, Conceptualization.

Declaration of competing interest

The authors declare the following financial interests/personal relationships which may be considered as potential competing interests: Shima Shahab reports financial support was provided by National Science Foundation. Arpit Agrawal reports financial support was provided by Lawrence Livermore National Laboratory. If there are other authors, they declare that they have no known competing financial interests or personal relationships that could have appeared to influence the work reported in this paper.

Data availability

Data will be made available on request.

Acknowledgment

This work was supported by the U.S. National Science Foundation (NSF) under the grant, Award No. CMMI 2016474, which is gratefully acknowledged. Arpit Agrawal would like to acknowledge the financial support and open access funding from Lawrence Livermore National Lab (LLNL).

Appendix A. Supplementary data

Supplementary data to this article can be found online at https://doi.org/10.1016/j.polymer.2024.127445.

References

[1] A. Lendlein, S. Kelch, Shape-memory polymers, Angew Chem. Int. Ed. Engl. 41 (12) (2002) 2035–2057.
[2] R. Xiao, J. Guo, D.L. Safranski, T.D. Nguyen, Solvent-driven temperature memory and multiple shape memory effects, Soft Matter 11 (20) (2015) 3977–3985.
[3] G. Li, G. Fei, H. Xia, J. Han, Y. Zhao, Spatial and temporal control of shape memory polymers and simultaneous drug release using high intensity focused ultrasound, J. Mater. Chem. 22 (16) (2012) 7692–7696.
[4] S. Zareie, A.S. Issa, R.J. Seethaler, A. Zabihollah, Recent advances in the applications of shape memory alloys in civil infrastructures: a review, Structures 27 (2020) 1535–1550.
[5] G. Costanza, M.E. Tata, Shape memory alloys for aerospace, recent developments, and new applications: a short review, Materials 13 (8) (2020).
[6] M. Asle Zaeem, N. Zhang, M. Mamivand, A review of computational modeling techniques in study and design of shape memory ceramics, Comput. Mater. Sci. 160 (2019) 120–136.
[7] Z.G. Wei, R. Sandstroröm, S. Miyazaki, Shape-memory materials and hybrid composites for smart systems: Part I Shape-memory materials, J. Mater. Sci. 33 (15) (1998) 3743–3762.
[8] Y. Zhao, Y. Chi, Y. Hong, Y. Li, S. Yang, J. Yin, Twisting for soft intelligent autonomous robot in unstructured environments, Proc. Natl. Acad. Sci. USA 119 (22) (2022) e2200265119.
[9] Y. Zhao, Y. Hong, F. Qi, Y. Chi, H. Su, J. Yin, Self-sustained snapping drives autonomous dancing and motion in free-standing wavy rings, Adv. Mater. 35 (7) (2023) 2207372.
[10] J. Delaey, P. Dubruel, S. Van Vlierberghe, Shape-memory polymers for biomedical applications, Adv. Funct. Mater. 30 (44) (2020) 1909047.
[11] L.M. Castano, A.B. Flatau, Smart fabric sensors and e-textile technologies: a review, Smart Mater. Struct. 23 (5) (2014) 053001.
[12] J. Xi, S. Shahab, R. Mirzaeifar, Qualifying the contribution of fiber diameter on the acrylate-based electrospun shape memory polymer nano/microfiber properties, RSC Adv. 12 (45) (2022) 29162–29169.
[13] Y. Liu, H. Du, L. Liu, J. Leng, Shape memory polymers and their composites in aerospace applications: a review, Smart Mater. Struct. 23 (2) (2014) 023001.
[14] Y. Zhao, K. Peng, J. Xi, S. Shahab, R. Mirzaeifar, Achieving multimodal locomotion by a crosslinked poly(ethylene-co-vinyl acetate)-based two-way shape memory polymer, Smart Mater. Struct. 31 (1) (2022) 015034.
[15] L. Song, W. Hu, G. Wang, G. Niu, H. Zhang, H. Cao, K. Wang, H. Yang, S. Zhu, Tailored (Meth)Acrylate shape-memory polymer networks for ophthalmic applications, Macromol. Biosci. 10 (10) (2010) 1194–1202.
[16] D. Rokaya, H.E. Skallevold, V. Srimaneepong, A. Marya, P.K. Shah, Z. Khurshid, M. S. Zafar, J. Sapkota, Shape memory polymeric materials for biomedical applications: an update, Journal of Composites Science 7 (2023), https://doi.org/10.3390/jcs7010024.
[17] C. Wang, M. Wang, S. Ying, J. Gu, Fast chemo-responsive shape memory of stretchable polymer nanocomposite aerogels fabricated by one-step method, Macromol. Mater. Eng. 305 (1) (2020) 1900602.
[18] S. Gopinath, N.N. Adarsh, P. Radhakrishnan Nair, S. Mathew, Recent trends in thermo-responsive elastomeric shape memory polymer nanocomposites, Polym. Compos. 44 (8) (2023) 4433–4458.
[19] S. Yang, Y. He, J. Leng, Regulated photo/thermal dual and programmable staged responsive shape memory poly(aryl ether ketone), J. Appl. Polym. Sci. 140 (38) (2023) e54444.
[20] F. Wang, M. Jiang, Y. Pan, Y. Lu, W. Xu, Y. Zhou, 3D Printing photo-induced lignin nanotubes/polyurethane shape memory composite, Polym. Test. 119 (2023) 107934.
[21] W. Huang, Y. Zhao, C. Wang, Z. Ding, H. Purnawali, C. Tang, J. Zhang, Thermo/chemo-responsive shape memory effect in polymers: a sketch of working mechanisms, fundamentals and optimization, J. Polym. Res. 19 (2012).
[22] C.M. Yakacki, R. Shandas, D. Safranski, A.M. Ortega, K. Sassaman, K. Gall, Strong, tailored, biocompatible shape-memory polymer networks, Adv. Funct. Mater. 18 (16) (2008) 2428–2435.
[23] A. Lendlein, M. Behl, B. Hiebl, C. Wischke, Shape-memory polymers as a technology platform for biomedical applications, Expet Rev. Med. Dev. 7 (3) (2010) 357–379.
[24] K. Gall, C.M. Yakacki, Y. Liu, R. Shandas, N. Willett, K.S. Anseth, Thermomechanics of the shape memory effect in polymers for biomedical applications, J. Biomed. Mater. Res. 73A (3) (2005) 339–348.
[25] Q. Ge, A.H. Sakhaei, H. Lee, C.K. Dunn, N.X. Fang, M.L. Dunn, Multimaterial 4D printing with tailorable shape memory polymers, Sci. Rep. 6 (1) (2016) 31110.
[26] H. Wu, P. Chen, C. Yan, C. Cai, Y. Shi, Four-dimensional printing of a novel acrylate-based shape memory polymer using digital light processing, Mater. Des. 171 (2019) 107704.
[27] J. Chowdhury, P.V. Anirudh, C. Karunakaran, V. Rajmohan, A.T. Mathew, K. Koziol, W.F. Alsanie, C. Kannan, A.S.S. Balan, V.K. Thakur, 4D printing of smart polymer nanocomposites: integrating graphene and acrylate based shape memory polymers, Polymers 13 (2021), https://doi.org/10.3390/polym13213660.
[28] X. Xiao, D. Kong, X. Qiu, W. Zhang, F. Zhang, L. Liu, Y. Liu, S. Zhang, Y. Hu, J. Leng, Shape-memory polymers with adjustable high glass transition temperatures, Macromolecules 48 (11) (2015) 3582–3589.
[29] Q. Xie, K. Fu, S. Liang, B. Liu, L. Lu, X. Yang, Z. Huang, F. Lü, Micro-structure and thermomechanical properties of crosslinked epoxy composite modified by nano-SiO2: a molecular dynamics simulation, Polymers 10 (2018), https://doi.org/10.3390/polym10070801.
[30] C.D. Wick, A.J. Peters, G. Li, Quantifying the contributions of energy storage in a thermoset shape memory polymer with high stress recovery: a molecular dynamics study, Polymer 213 (2021) 123319.
[31] D.L. Safranski, K. Gall, Effect of chemical structure and crosslinking density on the thermo-mechanical properties and toughness of (meth)acrylate shape memory polymer networks, Polymer 49 (20) (2008) 4446–4455.
[32] J. Xi, A. Sallam, D. Safranski, R. Mirzaeifar, S. Shahab, Hydrophilic and hydrophobic shape memory polymer networks in high-intensity focused ultrasound fields, Smart Mater. Struct. 33 (2) (2024), https://doi.org/10.1088/1361-665X/ad1d07.
[33] A. Bhargava, Dynamics of Smart Materials in High Intensity Focused Ultrasound Field, Virginia Tech, 2020.
[34] A. Bhargava, K. Peng, S. Shahab, Dynamics of focused ultrasound actuated shape memory polymers, Proc. SPIE 1096720 (2019), https://doi.org/10.1117/12.2514362.
[35] A. Bhargava, S. Shahab, Coupling of nonlinear shape memory polymer cantilever dynamics with focused ultrasound field, Smart Mater. Struct. 28 (5) (2019).
[36] A. Bhargava, K. Peng, J. Stieg, R. Mirzaeifar, S. Shahab, Focused ultrasound actuation of shape memory polymers; acoustic-thermoelastic modeling and testing, RSC Adv. 7 (72) (2017) 45452–45469.
[37] K. Peng, Y. Zhao, S. Shahab, R. Mirzaeifar, Ductile shape-memory polymer composite with enhanced shape recovery ability, ACS Appl. Mater. Interfaces 12 (52) (2020) 58295–58300.
[38] K. Peng, S. Shahab, R. Mirzaeifar, Interaction of high-intensity focused ultrasound with polymers at the atomistic scale, Nanotechnology 32 (4) (2020) 045707.
[39] K. Peng, R. Mirzaeifar, Interplay of chain orientation and bond length in size dependency of mechanical properties in polystyrene nanofibers, ACS Appl. Polym. Mater. 2 (4) (2020) 1664–1671.
[40] K. Peng, A. Nain, R. Mirzaeifar, Tracking the origins of size dependency in the mechanical properties of polymeric nanofibers at the atomistic scale, Polymer 175 (2019) 118–128.
[41] H. Ma, Z. Tian, Effects of polymer chain confinement on thermal conductivity of ultrathin amorphous polystyrene films, Appl. Phys. Lett. 107 (7) (2015) 073111.
[42] J. Diani, K. Gall, Molecular dynamics simulations of the shape-memory behaviour of polyisoprene, Smart Mater. Struct. 16 (5) (2007) 1575.
[43] J. Moon, J. Choi, M. Cho, Programmed shape-dependence of shape memory effect of oriented polystyrene: a molecular dynamics study, Polymer 102 (2016) 1–9.
[44] M. Amini, K. Hasheminejad, A. Montazeri, Experimentally guided MD simulation to enhance the shape memory behavior of polymer-based nanocomposites: towards

elaborating the underlying mechanism, Compos. Appl. Sci. Manuf. 138 (2020) 106055.
[45] W. Jian, X. Wang, H. Lu, D. Lau, Molecular dynamics simulations of thermodynamics and shape memory effect in CNT-epoxy nanocomposites, Compos. Sci. Technol. 211 (2021) 108849.
[46] D.S. Biovia, Materials Studio, 2019.
[47] P. Dauber-Osguthorpe, V.A. Roberts, D.J. Osguthorpe, J. Wolff, M. Genest, A. T. Hagler, Structure and energetics of ligand binding to proteins: Escherichia coli dihydrofolate reductase-trimethoprim, a drug-receptor system, Proteins 4 (1) (1988) 31–47.
[48] S. Plimpton, Fast Parallel algorithms for short-range molecular dynamics, J. Comput. Phys. 117 (1) (1995) 1–19.
[49] A. Stukowski, Visualization and analysis of atomistic simulation data with OVITO-the Open Visualization Tool, Model. Simulat. Mater. Sci. Eng. 18 (2010) 015012.
[50] P. Nourian, C.D. Wick, G. Li, A.J. Peters, Correlation between cyclic topology and shape memory properties of an amine-based thermoset shape memory polymer: a coarse-grained molecular dynamics study, Smart Mater. Struct. 31 (10) (2022) 105014.
[51] K. Duan, J. Zhang, L. Li, Y. Hu, W. Zhu, X. Wang, Diamond nanothreads as novel nanofillers for cross-linked epoxy nanocomposites, Compos. Sci. Technol. 174 (2019) 84–93.
[52] M.S. Radue, V. Varshney, J.W. Baur, A.K. Roy, G.M. Odegard, Molecular modeling of cross-linked polymers with complex cure pathways: a case study of bismaleimide resins, Macromolecules 51 (5) (2018) 1830–1840.
[53] T. Vo, B. Reeder, A. Damone, P. Newell, Effect of domain size, boundary, and loading conditions on mechanical properties of amorphous silica: a reactive molecular dynamics study, Nanomaterials 10 (2020), https://doi.org/10.3390/nano10010054.
[54] I.H. Sahputra, A.T. Echtermeyer, Effects of temperature and strain rate on the deformation of amorphous polyethylene: a comparison between molecular dynamics simulations and experimental results, Model. Simulat. Mater. Sci. Eng. 21 (6) (2013) 065016.
[55] X. Fu, Nanostructure, plastic deformation, and influence of strain rate concerning Ni/Al(2)O(3) interface system using a molecular dynamic study (LAMMPS), Nanomaterials 13 (4) (2023).
[56] D. Hossain, Others, Molecular dynamics simulations of deformation mechanisms of amorphous polyethylene, Polymer 51 (2010) 6071–6083.
[57] T.W. Sirk, K.S. Khare, M. Karim, J.L. Lenhart, J.W. Andzelm, G.B. McKenna, R. Khare, High strain rate mechanical properties of a cross-linked epoxy across the glass transition, Polymer 54 (26) (2013) 7048–7057.
[58] S. Afsharhashemkhani, M. Jamal-Omidi, M. Tavakolian, Investigation of strain rate effects on the mechanical behavior of polymer nanocomposites with and without defects in nanotubes, Polym. Bull. 80 (8) (2023) 8877–8898.
[59] H. Park, B. Kim, J. Choi, M. Cho, Influences of the molecular structures of curing agents on the inelastic-deformation mechanisms in highly-crosslinked epoxy polymers, Polymer 136 (2018) 128–142.
[60] A. Agrawal, R. Mirzaeifar, Computational investigation of deformation mechanisms at the atomistic scale of metallic glass-graphene composites (MGGCs), J. Appl. Phys. 130 (15) (2021) 155105.
[61] D. Leenaerts, W.M. Van Bokhoven, Piecewise Linear Modeling and Analysis, Springer Science & Business Media, 2013.
[62] M.K. Transtrum, J.P. Sethna, Improvements to the Levenberg-Marquardt Algorithm for Nonlinear Least-Squares Minimization, 2012 arXiv preprint arXiv:1201.5885.
[63] F. Syed, S. Zainuddin, A. Willis, M. Hosur, S. Jeelani, Crosslinking and interfacial behavior of carboxylic functionalized carbon nanotube Epon nanocomposites: a molecular dynamic simulation approach, SN Appl. Sci. 1 (11) (2019) 1423.
[64] M.A.F. Afzal, A.R. Browning, A. Goldberg, M.D. Halls, J.L. Gavartin, T. Morisato, T. F. Hughes, D.J. Giesen, J.E. Goose, High-throughput molecular dynamics simulations and validation of thermophysical properties of polymers for various applications, ACS Appl. Polym. Mater. 3 (2) (2021) 620–630.
[65] M. Hadipeykani, F. Aghadavoudi, D. Toghraie, A molecular dynamics simulation of the glass transition temperature and volumetric thermal expansion coefficient of thermoset polymer based epoxy nanocomposite reinforced by CNT: a statistical study, Phys. Stat. Mech. Appl. 546 (2020) 123995.
[66] J. Li, S. Jin, G. Lan, S. Chen, L. Li, Molecular dynamics simulations on miscibility, glass transition temperature and mechanical properties of PMMA/DBP binary system, J. Mol. Graph. Model. 84 (2018) 182–188.
[67] J. Han, R.H. Gee, R.H. Boyd, Glass transition temperatures of polymers from molecular dynamics simulations, Macromolecules 27 (26) (1994) 7781–7784.
[68] Q. Yang, X. Chen, Z. He, F. Lan, H. Liu, The glass transition temperature measurements of polyethylene: determined by using molecular dynamic method, RSC Adv. 6 (15) (2016) 12053–12060.
[69] J.S. Bermejo, C.M. Ugarte, Influence of cross-linking density on the glass transition and structure of chemically cross-linked pva: a molecular dynamics study, Macromol. Theory Simul. 18 (6) (2009) 317–327.
[70] J. Lawson, J. Monk, J. Haskins, C. Bauschlicher, Mechanical and thermal properties of cross-linked phenolic resins using molecular dynamics, APS March Meeting Abstracts (2013) C31.011.
[71] Z. Luo, Z. Yang, Z. Fei, K. Li, Effect of crosslinking rate on the glass transition temperature of polyimide cross-linked silica aerogels, J. Polym. Res. 27 (9) (2020) 255.
[72] M. Mansilla, A. Rodriguez Garraza, L. Silva, W. Salgueiro, C. Macchi, Á. Marzocca, A. Somoza, Evolution of the free volume and glass transition temperature with the degree of cure of polybutadiene rubbers, Polym. Test. 32 (2013) 686–690.
[73] J. Chua, Q. Tu, A molecular dynamics study of crosslinked phthalonitrile polymers: the effect of crosslink density on thermomechanical and dielectric properties, Polymers 10 (2018), https://doi.org/10.3390/polym10010064.
[74] H. Yang, Z. Wang, Y. Guo, X. Shi, *A molecular dynamics investigation of the deformation mechanism and shape memory effect of epoxy shape memory polymers.* Science China Physics, Mechanics & Astronomy 59 (3) (2016) 634601.
[75] X.L. Wu, S.F. Kang, X.J. Xu, F. Xiao, X.L. Ge, Effect of the crosslinking density and programming temperature on the shape fixity and shape recovery in epoxy–anhydride shape-memory polymers, J. Appl. Polym. Sci. 131 (15) (2014).
[76] K. Yu, Q. Ge, H.J. Qi, Reduced time as a unified parameter determining fixity and free recovery of shape memory polymers, Nat. Commun. 5 (1) (2014) 3066.
[77] B.C. Abberton, W.K. Liu, S. Keten, Coarse-grained simulation of molecular mechanisms of recovery in thermally activated shape-memory polymers, J. Mech. Phys. Solid. 61 (12) (2013) 2625–2637.